The Astrophysical Journal, 802:134 (7pp), 2015 April 1 doi:10.1088/0004-637X/802/2/134

POYNTING-FLUX-DOMINATED JETS CHALLENGED BY THEIR PHOTOSPHERIC EMISSION

D. Bégué[1,2,4] and A. Pe'er[3]
[1] Department of Physics, Royal Institute of Technology (KTH), AlbaNova, SE-106 91 Stockholm, Sweden
[2] The Oskar Klein Centre for Cosmoparticle Physics, AlbaNova, SE-106 91 Stockholm, Sweden
[3] Physics Department, University College Cork, Cork, Ireland
Received 2014 October 8; accepted 2015 February 3; published 2015 April 2

ABSTRACT

One of the key open question in the study of jets, in general, and jets in gamma-ray bursts (GRBs), in particular, is the magnetization of the outflow. Here we consider the photospheric emission of Poynting-flux-dominated outflows, when the dynamics is mediated by magnetic reconnection. We show that thermal three-particle processes, responsible for the thermalization of the plasma, become inefficient at a radius of $r_{\rm sup} \sim 10^{9.5}$ cm, far below the photosphere, at $\sim 10^{11.5}$ cm. Conservation of the total photon number above $r_{\rm sup}$ combined with Compton scattering below the photosphere enforces kinetic equilibrium between electrons and photons. This, in turn, leads to an increase in the observed photon temperature, which reaches $\gtrsim 8$ MeV (observed energy) when decoupling the plasma at the photosphere. This result is weakly dependent on the free model parameters. We show that in this case, the expected thermal luminosity is a few percent of the total luminosity, and could therefore be detected. The predicted peak energy is more than an order of magnitude higher than the observed peak energy of most GRBs, which puts strong constraints on the magnetization of these outflows.

Key words: gamma-ray burst: general – magnetic reconnection – plasmas – radiation mechanisms: thermal

1. INTRODUCTION

One of the key open questions in the study of relativistic outflows, in general, and of gamma-ray bursts (GRBs), in particular, is the mechanism responsible for accelerating the plasma to the ultra-relativistic speeds observed, $\Gamma \gtrsim 100$ (for a review, see, e.g., Mészáros 2006; Gehrels & Mészáros 2012; Zhang 2014). In the classical GRB "fireball" model (Paczynski 1986, 1990; Rees & Meszaros 1992, 1994; Piran et al. 1993), the outflow is accelerated by the radiative pressure of the photons produced during the initial phase of collapse and explosion. In this model, conservation of energy and entropy implies a linear increase of the jet Lorentz factor Γ with radius r until the jet reaches the saturation radius r_s, above which the jet internal energy is comparable to its kinetic energy, and no further acceleration is possible. In this model, magnetic fields are sub-dominant (the energy density stored in the magnetic field is much smaller than the energy density in the thermal photon field, $u_B \ll u_{\rm th}$).

On the other hand, it was proposed that GRB outflows are magnetically dominated, $U_B \gg U_{\rm th}$ (Spruit et al. 2001; Drenkhahn 2002; Drenkhahn & Spruit 2002; Lyutikov & Blandford 2003; Giannios 2006). In this scenario, if the central engine is able to produce a highly variable magnetic field, magnetic reconnection may be the mechanism responsible for the jet acceleration: the reconnection process results in a magnetic pressure gradient that accelerates the outflow. Under the assumption of a steady energy transfer rate, the most efficient configuration of magnetic line orientation leads to a slower increase in the bulk Lorentz factor with radius, $\Gamma \propto r^{1/3}$ below the saturation radius (Drenkhahn 2002; Drenkhahn & Spruit 2002; Mészáros & Rees 2011).

Since the magnetic field is not directly observed, one has to deduce its significance indirectly. For example, in their analysis of GRB080916C, Zhang & Pe'er (2009) argued that at least part of the outflow energy has to be in magnetic form. Their argument is based on the absence of a thermal component in the spectrum, which originates from the photosphere, and must accompany any photon-dominated outflow.

A different result was recently claimed by Bromberg et al. (2014). They argued that highly magnetized jets are disfavored by many GRB observations since they do not allow for the reproduction of the plateau in the distribution of the GRB duration. This is because Poynting-flux-dominated jets are stable and break the envelope of their progenitor star on a time that is significantly shorter than observed. In contrast, the break time of baryonic jets are in agreement with the duration of the observed plateau, favoring this last model.

Solving this controversy is indeed of high importance because the magnetization of the outflow puts strong constraints not only on possible acceleration mechanisms, but also on the nature of GRB progenitors, as well as the central engines that power GRBs. In this paper, we propose a novel way of constraining the magnetization of GRB outflows, based on their observed spectra. The key is the study of photon production processes. As we show here, models in which GRB jets are strongly magnetized lead to the suppression of photon production. The produced photons, in turn, are Compton upscattered; due to their small number, the predicted spectral peak is at $\gtrsim 8$ MeV, more than an order of magnitude above the typical observed peak.

2. DYNAMICS OF POYNTING-FLUX-DOMINATED JETS

The evolution of the hydrodynamic quantities in a Poynting-flux-dominated outflow was first derived by Drenkhahn (2002), Drenkhahn & Spruit (2002), and was further discussed by Giannios (2005, 2006), Giannios & Spruit (2005), Mészáros & Rees (2011). In this model, an important physical quantity is the magnetization parameter, σ_0, which is the ratio

[4] Erasmus Mundus Joint Doctorate IRAP PhD student.

of Poynting flux to kinetic energy flux at the Alfvén point, r_0.[5] This quantity plays a similar role to that of the baryon loading, in the classical "fireball" model.

The magnetic field in the flow changes polarity on a small scale, λ, which is of the order of the light cylinder in the central engine frame ($\lambda \approx 2\pi c/\Omega$, where Ω is the angular frequency of the central engine—presumably a spinning black hole; see Coroniti 1990). This polarity change leads to magnetic energy dissipation via the reconnection process that is modeled by a fraction ϵ of the Alfvén speed.[6]

The dissipated magnetic energy is converted to kinetic energy of the outflow, leading to a acceleration of the plasma. The spatial evolution of the Lorentz factor, Γ, and of the comoving number density, n_e', below the saturation radius r_s are given by

$$\Gamma(r) = \Gamma_\infty \left(\frac{r}{r_s}\right)^{1/3}, \tag{1}$$

$$n_e' = \frac{L}{m_p c^3 r^2 \Gamma(r)\left(\sigma_0 + 1\right)^{3/2}}, \tag{2}$$

where the terminal Lorentz factor $\Gamma_\infty \simeq \sigma_0^{3/2}$. The saturation radius is given by $r_s = \pi c \Gamma_\infty^2/(3\epsilon\Omega)$, where $\epsilon\Omega$ is the characteristic frequency of the reconnection process (Drenkhahn 2002). The outflow luminosity (both magnetic and kinetic per unit of solid angle str^{-1}) is $L = L_k + L_B = \dot{M}c^2(\sigma_0 + 1)^{3/2}$, where $\dot{M}$ is the outflow mass flux.

The spatial evolution of the comoving magnetic field, $B' = B/\Gamma$, can be calculated using Equation (1), the definition of the magnetic luminosity, $L_B = (B^2/4\pi)cr^2$, the definition of the saturation radius, and energy conservation $L = L_k + L_B$. Using $L_B(r) = L(1 - \Gamma(r)/\Gamma_\infty) = L(1 - \Gamma(r)/\sigma_0^{3/2})$ below the saturation radius (Giannios & Spruit 2005), one obtains

$$B' \equiv \frac{B}{\Gamma} = \left(\frac{4\pi L}{c}\right)^{1/2}\left(\frac{\pi c}{3}\right)^{1/3}\frac{1}{r^{4/3}\sigma_0^{1/2}(\epsilon\Omega)^{1/3}}\left[1 - \left(\frac{r}{r_s}\right)^{1/3}\right]^{1/2}$$
$$\approx 1.4 \times 10^8 \frac{L_{52}^{1/2}}{r_{11}^{4/3}(\epsilon\Omega)_3^{1/3}\sigma_2^{1/2}}\ \mathrm{G}, \tag{3}$$

where $r_s \gg r$ is taken in the last equality, and $Q = 10^x Q_X$ in cgs units is used here and below.

Deep enough in the flow, radiation and matter are in thermodynamic equilibrium, sharing the same temperature, T. The thermal energy increases by magnetic energy dissipation and simultaneously decreases due to adiabatic losses. As a consequence, only a fraction of the injected thermal energy appears as blackbody radiation at the photospheric radius where matter and radiation decouple.

The spatial evolution of the comoving temperature was calculated by Giannios & Spruit (2005), under the assumption of full thermalization. For completeness, we briefly repeat their arguments. For a constant magnetic energy dissipation rate, the energy released at radii $(r\,..\,r + dr)$ is

$$d\dot{E} = \left(-\frac{dL_B}{dr}\right)dr$$
$$= \frac{L}{3\sigma_0}\left(\frac{3}{\pi c}\right)^{1/3}(\epsilon\Omega)^{1/3} r^{-2/3} dr, \tag{4}$$

where we used the formula for L_B given above Equations (1) and (3), and the definition of r_s. About half of this dissipated energy is used to accelerate the flow, and the other half increases its thermal energy (Spruit & Drenkhahn 2004). Adiabatic losses in radiative-dominated flow imply $T' \propto n_e'^{1/3} \propto r^{-7/9}$, using Equation (2). Using again the scaling of the Lorentz factor in Equation (1), one obtains $L_{\rm th}(r) \propto r^2\Gamma^2 T'^4 \propto r^{-4/9}$. Therefore, by the time the plasma reaches some radius R, only a fraction $(r/R)^{4/9}$ of the energy dissipated at radius $r < R$ is still in thermal form. Integrating over all radii, the thermal luminosity at radius r is given by

$$L_{\rm th}(r) = \frac{1}{2}\int_{r_0}^{r} d\dot{E}\left(\frac{r'}{r}\right)^{4/9} dr'$$
$$= \frac{1}{2}\left(\frac{L}{3\sigma_0}\right)\left(\frac{3}{\pi c}\right)^{1/3}(\epsilon\Omega)^{1/3}\left(\frac{9}{7}\right)r^{1/3}. \tag{5}$$

The comoving temperature of the flow is calculated using $L_{\rm th} = \frac{16}{3}\sigma_{\rm SB} r^2 \Gamma^2 T'^4$, where $\sigma_{\rm SB}$ is the Stefan–Boltzmann constant and is given by

$$\theta' \equiv \frac{k_B T'}{m_e c^2}$$
$$= 1.4 \times 10^{-3}\frac{L_{52}^{1/4}}{r_{11}^{7/12}(\epsilon\Omega)_3^{1/12}\sigma_2^{1/2}}, \tag{6}$$

where we normalized the temperature to natural units of $m_e c^2$.

Photons decouple the plasma once they reach the photosphere, at which the optical depth becomes smaller than the unity. Along the radial direction, $d\tau = \Gamma(1 - \beta)n_e'\sigma_T dr$, where σ_T is Thomson's cross section. Integrating from $r_{\rm ph}$ to infinity and requiring $\tau(r_{\rm ph}) = 1$, using Equations (1) and (2), the photospheric radius is given by (Abramowicz et al. 1991; Giannios & Spruit 2005; Pe'er 2008)

$$r_{\rm ph} = 6 \times 10^{11}\frac{L_{52}^{3/5}}{(\epsilon\Omega)_3^{2/5}\sigma_2^{3/2}}\ \mathrm{cm}. \tag{7}$$

For the fiducial values of the free model parameters assumed, $\sigma_0 = 100$ and $(\epsilon\Omega) = 10^3$, this radius is below the saturation radius, $r_s \approx 10^{13.5}\,\sigma_2^3(\epsilon\Omega)_3^{-1}$ cm. This implies that the photons decouple the plasma while it is still in the acceleration phase.

The results of Equation (6) imply that as long as the photons maintain thermal equilibrium, their comoving number density scales with radius as $n_\gamma' \propto u_{\rm th}'/\langle\epsilon'\rangle \propto \theta'^4/\theta' \propto r^{-7/4}$. Here, $u_{\rm th}' = aT'^4$ is the comoving thermal energy density, and $\langle\epsilon'\rangle = 2.7 k_B T'$ is the average photon energy. If, however, photon production is suppressed above some radius $r_{\rm sup} < r_{\rm ph}$ (namely, the remaining photons are still coupled to the particles in the plasma), the scaling low $T' \propto r^{-7/9}$ derived above implies that the photon density changes with radius as $n_\gamma' \propto T'^3 \propto r^{-7/3}$. The photon number density in this case thus drops faster than in thermal equilibrium. These photons eventually decouple the plasma at the photosphere. As we show below, this different scaling law modifies the emerging

[5] In Poynting-flux-dominated models, at r_0 the flow velocity is equal to the Alfvén speed. Acceleration takes place at $r_0 < r < r_s$, where r_s is the saturation radius.

[6] Note that this prescription assumes a constant rate of energy transfer along the jet. As the details of the reconnection process are uncertain, the value of ϵ is highly uncertain. Often a constant value of $\epsilon \approx 0.1$ is assumed in the literature. Furthermore, note that the Alfvén speed is essentially equal to the speed of light in magnetically dominated outflows.

spectra at the photosphere, and in particular the observed peak energy.[7]

3. PHOTON PRODUCTION MECHANISMS

In the following, we consider photon production below the photosphere. The leading radiative processes are double Compton, bremsstrahlung, and cyclo-synchrotron. Other radiative mechanisms, such as radiative pair production and three-photon annihilation are discarded because the plasma is not relativistic ($\theta' < 1$, see Equation (6)).

The key question is whether the photon sources are capable of producing enough photons to enable full thermalization below the photosphere. The rate of the interactions considered below were discussed by Beloborodov (2013) and Vurm et al. (2013) and references therein. For each of these processes, the radius at which a given interaction freezes out is given by equating the photon production rate $\dot{n}$ to the expansion rate,

$$t_{\rm exp}\dot{n} \geqslant n_{\gamma,{\rm th}} \tag{8}$$

where $t_{\rm exp} = r/(c\Gamma(r))$ and $n_{\gamma,{\rm th}} = 16\pi\zeta(3)(k_BT')^3/(ch)^3$ is the photon number density obtained if the photons are in thermal equilibrium ($\zeta(3) \approx 1.202$ is the Riemann zeta function and h is Planck's constant).

Double Compton. The rate of photon production in a double Compton process is given by (Lightman 1981)

$$\dot{n}_{\rm DC} = \frac{16\alpha}{\pi} c\sigma_T \theta'^2 g_{\rm DC}(\theta') \ln\left(\frac{k_BT'}{E_0}\right) n'_e n_{\gamma,{\rm th}}, \tag{9}$$

where α is the fine-structure constant, $g_{\rm DC}(\theta') = (1+13.91\theta' + 11.05\theta'^2 + 19.92\theta'^3)^{-1} \approx 1$ is a fitted formula to the exact numerical result (Svensson 1984) and E_0 is the threshold energy.[8] Using Equations (8) and (9), the radius R_{DC} at which double Compton freezes out is

$$R_{\rm DC} = 2.4 \times 10^9 L_{52}^{\frac{9}{17}} \sigma_2^{-\frac{21}{17}} (\epsilon\Omega)^{-\frac{5}{17}} \ {\rm cm}. \tag{10}$$

Bremsstrahlung. The temperature at which bremsstrahlung freezes out is not relativistic, hence the pair density is expected to be much smaller than the proton density. As a consequence, the dominant bremsstrahlung process is scattering between electrons and protons. The rate of photon production via $e-p$ bremsstrahlung can be derived, e.g., using formula (5.14) in (Rybicki & Lightman 1979). Dividing by $h\nu$ and using the normalized photon energy $x \equiv h\nu/m_ec^2$, the photon emission rate per unit volume per unit energy is $d\dot{n}/dx = (8/3\pi)^{1/2} c\sigma_T \alpha n_e'^2 \theta'^{-1/2} x^{-1} \bar{g}_{ff}$, where the Gaunt factor can be approximated by $\bar{g}_{ff} \simeq (\sqrt{3}/\pi)\ln(2.25\theta/x)$ (Novikov & Thorne 1973; Illarionov & Siuniaev 1975; Pozdnyakov et al. 1983). The total photon emission rate is calculated by integrating over all energies, from $x = x_{\rm min}$ to $x = \theta$,

$$\dot{n}_B = \frac{\sqrt{2}}{\pi^{3/2}} c\sigma_T \alpha \theta'^{-1/2} n_e'^2 \times \left[\ln\left(2.25\frac{\theta'}{x_{\rm min}}\right)^2 - \ln(2.25)^2\right]. \tag{11}$$

The lower boundary on the energy of emitted photons, $x_{\rm min}$, is found by comparing the absorption time, $(\alpha_{ff}c)^{-1}$, to the typical time a photon gains sufficient energy (by inverse Compton scattering) to avoid re-absorption, $4\theta' nc\sigma_T$ (Vurm et al. 2013). Using the standard formula for free–free absorption in the Rayleigh–Jeans limit, $x_{\rm min}$ is calculated by solving

$$x_{\rm min}^2 = \frac{1}{8\sqrt{2}\pi^{5/2}} \alpha \lambda_c^3 n' \theta'^{-5/2} \ln \times \left(2.25\frac{\theta'}{x_{\rm min}}\right), \tag{12}$$

where $\lambda_c = h/m_ec$ is the Compton wavelength. While an analytic solution to this equation does not exist, it is easily checked numerically that for a wide range of relevant parameter space, $10^{-4} \lesssim x_{\rm min} \lesssim 10^{-3}$, leading to $\bar{A} \equiv \ln(2.25\theta'/x_{\rm min})^2 - \ln(2.25)^2 \simeq 15$.

Using these results in Equation (8) enables us to calculate the radius at which bremsstrahlung freezes out. For $\sigma_0 \gg 1$, this radius is approximated by

$$R_B \simeq 2.47 \times 10^9 \left(\frac{\bar{A}}{15}\right)^{\frac{24}{47}} L_{52}^{\frac{27}{47}} (\epsilon\Omega)_3^{\frac{7}{47}} \sigma_2^{-\frac{30}{47}} \ {\rm cm}. \tag{13}$$

Cyclo-synchrotron. The rate of photon emission via cyclo-synchrotron process from a thermal population of electrons is given by (Vurm et al. 2013 and references therein)

$$\dot{n}_{\rm CS} = \frac{12\pi m_e}{h^3} \sigma_T n'_e \theta'^2 \hat{E}_0^{\ 2}, \tag{14}$$

where $\hat{E}_0$ is the energy at which up-scattering and re-absorption rates are equal. For $\theta' \ll 1$, $\hat{E}_0$ can be approximated by (Vurm et al. 2013)

$$\hat{E}_0 = 14\left(\frac{m_ec^2}{E_B}\right)^{1/10} \theta'^{3/10} E_B, \tag{15}$$

where $E_B = hqB'/(2\pi m_ec)$ is the cyclotron energy in the comoving frame. Assuming $\sigma_0 \gg 1$, and using the equations above, one finds that the freeze-out radius for cyclo-synchrotron emission is

$$R_{\rm CS} = 5.50 \times 10^9 L_{52}^{\frac{54}{115}} (\epsilon\Omega)_3^{-\frac{37}{115}} \sigma_2^{-\frac{96}{115}} {\rm cm}. \tag{16}$$

While in the derivation of Equation (16) we assumed a thermal population of electrons, we do not expect this result to change if electrons are accelerated to high energies during the dissipation process (see, e.g., Sironi & Spitkovsky 2014). This is due to the fact that the typical energy of a synchrotron emitted photon is proportional to $\gamma_{\rm el}^2$, where $\gamma_{\rm el}$ is the Lorentz factor associated with the random motion of the electrons, and the total radiated power is similarly proportional to $\gamma_{\rm el}^2$. Thus, the rate of photon emission is independent of $\gamma_{\rm el}$.

[7] We note that in the classical "fireball" model dynamics, where magnetic fields are sub-dominant, this does not hold: even if photon production is suppressed above a certain radius, the scaling laws of the photon number density below the photosphere is not affected.

[8] A photon of energy $E > E_0$ will be up-scattered to higher energy by single Compton scattering and avoid re-absorption by the inverse process. E_0 is found by equating the Compton parameter $y = 4\theta' c\sigma_T n'$ to the photon opacity. For the double Compton process, E_0 is such that $(E_0/k_BT')^2 = 9.6\alpha\theta' g_{\rm DC}(\theta')/\pi$.

All radiative processes freeze out at $r_{\rm sup} = \max(R_{\rm CD}, R_B, R_{\rm CS})$. For the fiducial values of the luminosity, magnetization, and angular frequency, Equations (7), (9), (13), and (16) imply $r_{\rm sup} \ll r_{\rm ph}$. As a result, thermal equilibrium can exist only at radii $r \leqslant r_{\rm sup}$. Above this radius, photons are not emitted at a high enough rate to ensure full thermalization. However, below the photosphere, Compton scattering enforces kinetic equilibrium between electrons and photons, such that both components can be described by a single temperature. The photon distribution at $r_{\rm sup} < r < r_{\rm ph}$, therefore, obeys Wien statistics.

4. CONSEQUENCES OF PHOTON STARVATION

The results of the previous section imply that to a good approximation, one can assume that at $r > r_{\rm sup}$ the total number of photons is conserved. The photons thus follow a Wien distribution, with average (co-moving) photon energy $\langle \epsilon' \rangle \sim 3k_B T'$. Due to the strong coupling between photons and electrons below the photosphere, the comoving thermal energy $u'_{\rm th}$ is shared by the protons, electrons, and photons. As the plasma is non-relativistic, the energy density at $r = r_{\rm sup}$ is $u'_{\rm th}(r_{\rm sup}) = 3k_B T'_{\rm sup}(n'_e + n_\gamma)$, where $T'_{\rm sup} = T'(r = r_{\rm sup})$, and the electron and photon densities are evaluated at $r_{\rm sup}$.

At larger radii, $r \geqslant r_{\rm sup}$, full thermalization cannot be achieved. Nonetheless, due to the strong coupling between electrons and photons, for radii not much above $r_{\rm sup}$ (see below) the photon distribution is close to thermal, with comoving temperature given by $k_B T'(r) = u'_{\rm th}(r)/3(n'_e(r) + n_\gamma(r))$. The energy density is $u'_{\rm th}(r) = L_{\rm th}(r)/(4/3)r^2\Gamma^2(r)c$[9], with $L_{\rm th}(r)$ given in Equation (5). Conservation of the photon number at $r > r_{\rm sup}$ implies that the comoving number density evolves according to $n_\gamma(r > r_{\rm sup}) = n_\gamma(r_{\rm sup})(r_{\rm sup}/r)^2[\Gamma(r_{\rm sup})/\Gamma(r)]$. For $n_\gamma \gg n'_e(r)$, one therefore obtains $T'(r) \propto L_{\rm th}(r)/\Gamma(r) \propto r^0$, namely $T'(r > r_{\rm sup}) = T'_{\rm sup}$.

The electrons are continuously heated by the magnetic reconnection process above $r_{\rm sup}$ (see Equation (4)). They simultaneously radiate their energy by synchrotron emission and inverse-Compton scattering the quasithermal photons. As long as the cooling rate is sufficiently high, efficient energy transfer between electrons and photons exists, and both populations can be characterized by (quasi-) thermal distributions with similar temperatures, $T'_{\rm sup}$. However, as the jet expands, the cooling rate decreases, and as a result, above some radius, r_c ($r_{\rm sup} < r_c < r_{\rm ph}$; see below) the cooling cannot balance the heating. At this stage, a "two-temperature plasma" is formed, with $T'_{\rm el} > T'_{\rm ph} \sim T'_{\rm sup}$ (see a detailed discussion in Pe'er et al. 2005, 2006).

The radius r_c at which radiative cooling balances heating is calculated as follows. The rate $\dot{E}$ of energy transfer via magnetic reconnection to the plasma as it expands from the radius r to $r + dr$ was calculated in Equation (4). We assume that about half of this energy is used to heat the particles (the other half is converted to kinetic energy), implying that the comoving energy gain rate per unit volume is $P'_{\rm heat} = (1/2)d\dot{E}/(cdV')$, where $dV' = \Gamma(r)r^2 dr$.[10] Assuming next that a fraction $f \leqslant 1$ of this energy is used to heat the electrons (rather than protons), using Equations (1) and (4) the electron heating rate is given by (Giannios 2006)

$$P'_{\rm rec} = \frac{fL}{6r^3\sigma_0^{3/2}} \sim 1.67 \times 10^{15} f_0 L_{52} r_{11}^{-3} \sigma_2^{-3/2} \,{\rm erg\ cm^{-3}\ s^{-1}}. \quad (17)$$

The main radiative loss term of the electrons is Compton scattering the thermal photons.[11] As the plasma is non-relativistic $(\gamma\beta)^2 \simeq 3k_B T'/(m_e c^2)$, and the power loss (per unit volume) at $r > r_{\rm sup}$ is thus $P'_{IC} = 4\sigma_T k_B T'_{\rm sup} n'_{\rm el} u'_{\rm th}/m_e c$ (where we assume that the thermal energy is dominated by the photons at r_c). Equating the energy loss and the energy gain rates gives

$$r_c = \begin{cases} 2.0 \times 10^{11} L_{52}^{\frac{48}{85}} f_0^{-\frac{3}{5}} (\epsilon\Omega)_3^{-\frac{59}{170}} \sigma_2^{-\frac{93}{68}} {\rm cm}, & ({\rm DC}) \\ 2.1 \times 10^{11} L_{52}^{\frac{129}{235}} f_0^{-\frac{3}{5}} (\epsilon\Omega)_3^{\frac{117}{235}} \sigma_2^{-\frac{18}{235}} \left(\frac{\bar{A}}{15}\right)^{-\frac{42}{235}} {\rm cm}, & ({\rm Brem.}) \\ 1.5 \times 10^{11} L_{52}^{\frac{1347}{2300}} f_0^{-\frac{3}{5}} (\epsilon\Omega)_3^{-\frac{194}{575}} \sigma_2^{-\frac{867}{575}} {\rm cm}, & ({\rm CS}) \end{cases} \quad (18)$$

when considering double Compton, bremsstrahlung, and cyclo-synchrotron, respectively, as the main photon production processes. We can thus conclude that for the fiducial values of the free model parameters chosen, $r_c < r_{\rm ph}$ in all scenarios considered.

At radii $r_c \leqslant r \leqslant r_{\rm ph}$, the electrons can no longer efficiently convert their gained energy to the photons.[12] The photon temperature thus freezes.[13] The peak of the observed spectrum (νF_ν) can, therefore, be estimated as follows. First, as the photons conserve their Wien distribution, the (comoving) peak energy is slightly above the average photon temperature, $E'_p = (4/3)\langle \epsilon' \rangle = 4k_B T'_{\rm sup}$. Second, due to the Lorentz boost, the observed energy of the photons that decouple the plasma at the photosphere is $E^{\rm ob}_{\rm pk} \simeq 2\Gamma(r_{\rm ph})E'_p$ (for the on-axis observer). The peak of the observed νF_ν spectrum is therefore expected at $E^{\rm ob}_p = 8\Gamma(r_{\rm ph})k_B T'_{\rm sup}$, namely

$$E^{\rm ob}_{\rm pk} = \begin{cases} 13.1\, L_{52}^{-\frac{1}{17}} (\epsilon\Omega)_3^{\frac{43}{102}} \sigma_2^{\frac{49}{68}}\ {\rm Mev}, & ({\rm DC}) \\ 12.9\, L_{52}^{-\frac{4}{47}} \sigma_2^{\frac{41}{47}} (\epsilon\Omega)_3^{\frac{70}{141}} \left(\frac{\bar{A}}{15}\right)^{-\frac{14}{47}} {\rm MeV}, & ({\rm Brem.}) \\ 8.1\, L_{52}^{-\frac{11}{460}} (\epsilon\Omega)_3^{\frac{151}{345}} \sigma_2^{\frac{56}{115}}\ {\rm Mev}. & ({\rm CS}). \end{cases} \quad (19)$$

Note the weak dependence on the luminosity L and on $\epsilon\Omega$, and the moderate dependence on the magnetization, σ.

The electron and photon temperatures are presented in Figures 1 and 2. In Figure 1, we present the spatial evolution of the comoving electron temperature. At $r < r_{\rm sup}$, the electrons temperature decays, in accordance to Equation (6). At larger radii, $r_{\rm sup} < r < r_c$, photon starvation leads to constant temperature, and at even larger radii it increases. For

[9] We omit the factor π in the denominator, as $L_{\rm th}(r)$ is the luminosity per steradian.

[10] The factor 4π is omitted since $d\dot{E}$ is already expressed in ${\rm str}^{-1}$.

[11] At all radii, the photon energy density, $u'_{\rm th} > u_B$.

[12] It can easily be checked by integrating from r_c to infinity that the Compton Y parameter in this regime is of the order of unity (e.g., Bégué Siutsou & Vereshchagin 2013).

[13] The photon temperature slightly increases below the photosphere due to Compton scattering with the electrons. However, this effect is discarded in our computation, since it only increases the observed temperature.

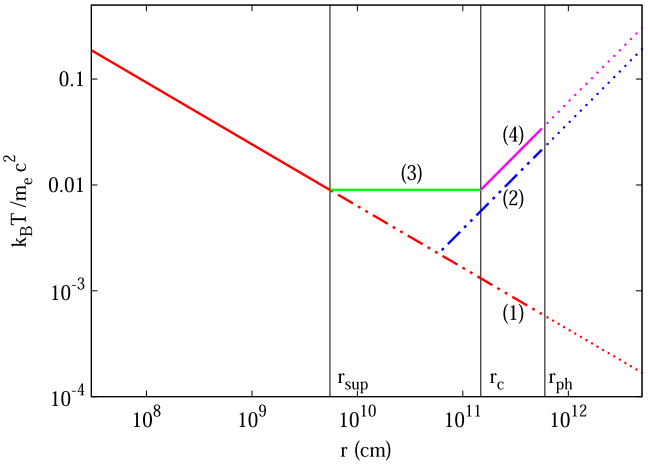

Figure 1. Radial evolution of the co-moving electron's temperature for the fiducial parameters $L_{52} = 1$, $\sigma_{0,2} = 1$ and $(\epsilon\Omega)_3 = 1$. Four segments are shown. (1) At small radii, the temperature is directly associated to the internal energy, and $T' \propto r^{-7/12}$ (see Equation (6)). (2) At $r > r_c$, coupling between the electrons and photons is weak, resulting in inefficient electron cooling which, in turn, leads to an increase of the electrons temperature. (3) When photon starvation is considered, the electron's temperature is fixed at $r_{sup} < r < r_c$, $T' = T'_{sup}$. (4) Same as in segment (2), but when photon starvation is taken into account. Thus, we expect the temperature to evolve along segments (1)–(3)–(4) (solid lines), with dashed–dotted lines (including segment (2)) for comparison only. With the parameters at hand, r_{sup} is given by the cyclo-synchrotron process.

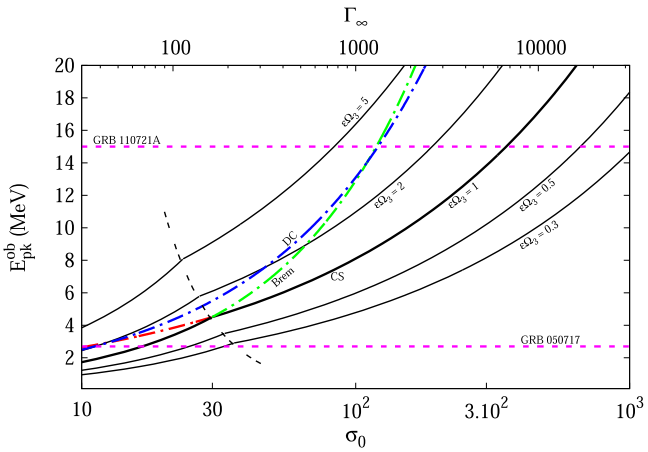

Figure 2. Observed peak energy as a function of the magnetization σ_0 for $L_{52} = 1$ and different reconnection frequencies $(\epsilon\Omega)_3$. The fiducial value $(\epsilon\Omega)_3 = 1$ is shown by the thick solid line, and other solid lines are for different values of $(\epsilon\Omega)_3$, as indicated. The double dashed thin (black) line shows the separation between photon production domination by the bremsstrahlung process at low σ_0 and cyclo-synchrotron domination at higher values of σ_0. The expected peak energy for $(\epsilon\Omega)_3 = 1$ via the different processes: bremsstrahlung, double Compton and cyclo-synchrotron are represented by the thick dashed–dotted lines (green, blue, and red, respectively). For comparison, we add the observed peak energies of the two highest record GRBs, GRB 050717, and GRB 110721A, by the two horizontal dashed (purple) lines.

comparison, we show the results obtained when photon starvation is omitted, which is shown by segments (1) and (2) (dashed–dotted lines) in Figure 1. In this case, the temperature continues to decay at radii $r > r_{sup}$, in accordance with Equation (6) (segment (1)). At larger radii the temperature increases again (segment (2)), once the electrons cannot efficiently convert their gained energy to the photons.

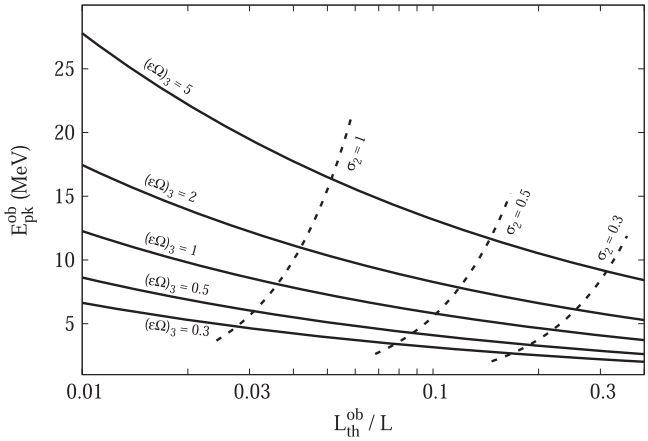

Figure 3. Peak energy E_{pk}^{ob} is plotted against the ratio of thermal to nonthermal luminosity, (L_{th}^{ob}/L) for different values of σ_2 and of $(\epsilon\Omega)$. The solid lines represent different values of σ for fixed values of $(\epsilon\Omega)_3$, ranging from 0.3 to 5. The dashed lines represent different values of $(\epsilon\Omega)_3$ for constant σ_2, ranging from 0.3 to 1. Here we consider $L_{52} = 1$, however, as both E_{pk}^{ob} and L_{th}^{ob}/L are weakly dependent on L, the result is not substantially different for other values of L_{52}.

The dependence of the observer (photon) temperature E_{pk}^{ob} on the unknown magnetization parameter σ is displayed in Figure 2. As is shown, for any value of $\sigma > 10$, the observed peak energy is greater than a few MeV, comparable only with the highest GRB peak energies observed. For comparison, we provide two examples: GRB 050717 having $E_{pk}^{ob} \sim 2.7$ MeV (Krimm et al. 2006) requires σ_0 to be at most of the order of 20. On the other hand, the extreme peak energy of the first seconds of GRB 110721A around 15 MeV (Axelsson et al. 2012) can be explained in a highly magnetized jet, having $\sigma_0 \sim 350$ for $(\epsilon\Omega)_3 = 1$. We stress though that these results show that the vast majority of GRBs, having peak energy at <MeV, are inconsistent with having a high magnetization parameter, $\sigma >$ a few, at least below the photosphere.

Within the framework of our model, a lower limit on the luminosity of the photosphere is derived by considering the thermal luminosity at r_c, as Compton scattering of photons above r_c only increases the photospheric luminosity. One obtains

$$L_{th}^{ob} > \begin{cases} 4.0 \times 10^{50} L_{52}^{\frac{101}{85}} (\epsilon\Omega)_3^{\frac{37}{170}} \sigma_2^{-\frac{99}{68}} f_0^{-\frac{1}{5}} \text{ erg s}^{-1}, & \text{(DC)} \\ 4.0 \times 10^{50} L_{52}^{\frac{278}{235}} (\epsilon\Omega)_3^{\frac{352}{705}} \sigma_2^{-\frac{241}{235}} f_0^{-\frac{1}{5}} \left(\frac{\bar{A}}{15}\right)^{-\frac{14}{235}} \\ \qquad \text{erg s}^{-1}, & \text{(Brem.)} \\ 3.6 \times 10^{50} L_{52}^{\frac{2749}{2300}} (\epsilon\Omega)_3^{\frac{127}{575}} \sigma_2^{-\frac{864}{575}} f_0^{-\frac{1}{5}} \text{ erg s}^{-1}. & \text{(CS)} \end{cases} \quad (20)$$

Thus, we conclude that the thermal part of the spectrum should be at least a few percent of the total burst luminosity. In fact, since the nonthermal part is spectrally broad, it is possible that if observing over a limited band, that the thermal component will carry a larger fraction of the observed luminosity than presented here. Such a component, although weak, may be detected by careful analysis. Finally, note that for GRB 110721A the expected fraction thermal luminosity is expected to be very small, of the order of 0.5% of the total luminosity.

The relation between $L_{\rm th}^{\rm ob}/L$ and $E_{\rm pk}^{\rm ob}$ as a function of σ_0 at constant $(\epsilon\Omega)$ is shown in Figure 3. The higher the photospheric peak (corresponding to large σ_0), the smaller the radiative efficiency of the photosphere.

5. DISCUSSION

In this work, we analyzed the expected photospheric signal from Poynting-flux-dominated outflows. As we show here, in these conditions full thermalization can only be achieved at small radii, $r < r_{\rm sup} \ll r_{\rm ph}$. As a result of this photon starvation, the observed νF_ν peak of the photospheric emission is expected above 8 MeV (see Equation (19)). Moreover, we find that this value has only weak dependence on the unknown values of the outflow parameters. This value is inconsistent with the observed peak energy of the vast majority of GRBs, which is of the order of 350 keV on average (Ghirlanda et al. 2009; Goldstein et al. 2012) for time-integrated spectra and rises up to 3 MeV in some exceptional cases. Thus, if this peak is due to emission from the photosphere, our results indicate that only bursts with the highest νF_ν peak might be marginally consistent with the photospheric emission of magnetically dominated outflows.

The understanding of GRB prompt emission has been revolutionized in the past few years, with evidence for thermal emission being widely accepted in many bursts (Ryde & Pe'er 2009; Ryde et al. 2010; Guiriec et al. 2011, 2013; Axelsson et al. 2012; Iyyani et al. 2013). Still, a full understanding of the origin of the spectra and the outflow conditions (in particular, the magnetization) are far from being understood. One hint may be the $E_{\rm pk}-E_{\rm iso}$ correlation (the "Amati" correlation; Amati et al. 2002; Amati 2006) that shows that high spectral peak energy correlates with high total energy release. Moreover, there is some evidence for high efficiency in the prompt emission in very energetic bursts (Lloyd-Ronning & Zhang 2004; Pe'er et al. 2012). It was proposed that these results may indicate a photospheric origin of a substantial part of the observed spectra, including the peak itself (Thompson et al. 2007; Lazzati et al. 2013; Deng & Zhang 2014). The results obtained here show, however, that if the flows are highly magnetized, the expected peak energy is too high to be consistent with the observed one, and the efficiency of photospheric emission is only a few percent (Equation (20)).

Our results indicate a high energy peak, at $\gtrsim$8 MeV, which is significantly higher than considered by Giannios (2006, 2012). This difference originates from the larger comoving temperature at r_c obtained here, resulting from photon starvation. They are aligned with the results obtained by Beloborodov (2013), which were considerably less detailed, and were obtained under the assumption of initially similar thermal and kinetic luminosity. It thus implies that the ratio of the photon number density to the electron number density is over-estimated.[14]

Alternatively, the photospheric emission may be sub-dominant, the dominant part of the prompt spectrum being nonthermal. However, in this case, the expected peak, at $\gtrsim$8 MeV, should contain a few percent of the burst luminosity, and should therefore be observed. Moreover, Beniamini & Piran (2014) studied jets in which the ratio of the Poynting luminosity to the total luminosity is large at the dissipation zone. By identifying the MeV peak with synchrotron emission, they found strong constraints on the dissipation radius and the Lorentz factor at the emission region. We thus conclude that magnetized jet models in which the photospheric component is sub-dominant have additional difficulties with explaining the observed spectra.

High magnetization implies a lower ratio of $L_{\rm th}/L$ (see Equation (20)). Thus, the non-detection of a thermal component may be a signal of highly magnetized outflow. Our results are therefore consistent with the previous analysis by Zhang & Pe'er (2009) and by Gao & Zhang (2014), and stress the need for a careful spectral analysis that could enable us to constrain the magnetization of GRB outflows.

The conditions for thermalization of the plasma in the classical "fireball" (when Poynting flux is sub-dominant) were studied by Vurm et al. (2013). In this work, it was shown that in order to obtain full thermalization, the energy dissipation radius is limited to a relatively narrow range ($r \sim 10^{10} - 10^{11}$cm), and the Lorentz factor during the dissipation must be mild, $\Gamma \sim 10$. Interestingly, these results are aligned with the inferred values of the outflow parameters (Pe'er et al. 2007).

In this manuscript, we considered jet acceleration via the magnetic reconnection process first proposed by Drenkhahn (2002) and Drenkhahn & Spruit (2002). In recent years, several new models of magnetized jets were proposed in the literature. Narayan et al. (2007) and Tchekhovskoy et al. (2008) considered self-similar solutions of strongly magnetized outflows in the force-free approximation. In these models, the magnetic field is attached to the (newly formed) accretion disk. A split-monopole solution was considered by Tchekhovskoy et al. (2009), and the effect of the collapsing star on highly magnetized jet dynamics was considered by Tchekhovskoy et al. (2010).

In these models, the acceleration is due to the spreading of magnetic lines, resulting in a pressure gradient, which accelerates the flow. Analytic estimates, confirmed by numerical integration of the MHD equations, show that the Lorentz factor increases proportionally to $\Gamma \propto r^\delta$, with $1/3 \leqslant \delta \leqslant 1$ (the model by Tchekhovskoy et al. 2010 result in a slower acceleration, $\Gamma \propto \log(r)^{1/3}$). The acceleration rate is not necessarily steady, in which case the Lorentz factor can be approximated by a broken power law. On the other hand, the laboratory magnetic field intensity decreases proportionally to $B \propto r^{-\delta}$.

As each individual model predicts a different acceleration scaling law, in order to obtained the expected photospheric signal, a full analysis is, in principle, required; however, such an analysis is beyond the scope of this manuscript, and is left for future work. Nonetheless, we can estimate the expected effect, by considering one model, that of Tchekhovskoy et al. (2008). We estimate the freeze-out radius of the cyclo-synchrotron process with $\delta = 0.5$. Considering Equations (A11), (A38), and (A45) of Tchekhovskoy et al. (2008)[15],

[14] Beloborodov (2013) estimated $E_{\rm pk}^{\rm ob} \simeq 3$ MeV, somewhat less than the results derived here. The origin of this discrepancy is his assumption of coasting Lorentz factor below the photosphere.

[15] Equation (A11) determines the shape of a field line; Equation (A38) gives the Lorentz factor of the fluid along a field line, and Equation (A45) gives the toroidal (dominant) component of the magnetic field B_ψ (see Tchekhovskoy et al. 2008 for details).

using Equations (8) and (14) derived above, we obtain

$$R_{\rm CS} \sim 7.12 \times 10^{10} \frac{L_{52}^{1/2}}{\sigma_2^{15/38} \Omega_3^{5/19} \theta_1^{2/19}} \ {\rm cm}, \quad (21)$$

where θ_1 is the plasma temperature after dissipation, normalized to 10 keV. We further find that R_{CS} strongly increases with increasing δ. Similarly, as the Lorentz factor increases faster with larger values of δ, the photospheric radius decreases. Thus, we can conclude that larger δ (faster acceleration) reduces the excluded parameter space region (namely, the parameter space region in which full thermalization cannot be obtained). This should lead to a decrease in the temperature of photospheric photons, with increasing values of δ. However, as we stated above, we leave a full qualitative study of this regime to future works.

In the magnetized outflow scenario considered here, the dissipation results from magnetic reconnection and is assumed to be continuous along the jet. Thus, one cannot constrain a particular dissipation radius. The approach taken here is therefore different: by prescribing the dynamics, we study its observational consequences, in particular, the expected peak energy and efficiency of the photospheric emission.

We are thankful to D. Giannios and B. Zhang for their useful comments. D.B. is supported by the Erasmus Mundus Joint Doctorate Program by grant No. 2011-1640 from the EACEA of the European Commission and acknowledges financial support from Stiftelsen Olle Engkvist Byggmästare. A.P. acknowledges support by Marie Curie grant FP7-PEOPLE-2013-CIG #618499.

REFERENCES

Abramowicz, M. A., Novikov, I. D., & Paczynski, B. 1991, ApJ, 369, 175
Amati, L. 2006, MNRAS, 372, 233
Amati, L., Frontera, F., Tavani, M., in't Zand, J. J. M., Antonelli, A., et al. 2002, A&A, 390, 81
Axelsson, M., Baldini, L., Barbiellini, G., Baring, M. G., Bellazzini, R., et al. 2012, ApJL, 757, L31
Bégué, D., Siutsou, I. A., & Vereshchagin, G. V. 2013, ApJ, 767, 139
Beloborodov, A. M. 2013, ApJ, 764, 157
Beniamini, P., & Piran, T. 2014, MNRAS, 445, 3892
Bromberg, O., Granot, J., & Piran, T. 2014, arXiv:1407.0123
Coroniti, F. V. 1990, ApJ, 349, 538
Deng, W., & Zhang, B. 2014, ApJ, 785, 112
Drenkhahn, G. 2002, A&A, 387, 714
Drenkhahn, G., & Spruit, H. C. 2002, A&A, 391, 1141
Gao, H., & Zhang, B. 2014, arXiv,1409.3584
Gehrels, N., & Mészáros, P. 2012, Science, 337, 932
Ghirlanda, G., Nava, L., Ghisellini, G., Celotti, A., & Firmani, C. 2009, A&A, 496, 585
Giannios, D. 2005, A&A, 437, 1007
Giannios, D. 2006, A&A, 457, 763
Giannios, D. 2012, MNRAS, 422, 3092
Giannios, D., & Spruit, H. C. 2005, A&A, 430, 1
Goldstein, A., Burgess, J. M., Preece, R. D., Briggs, M. S., Guiriec, S., et al. 2012, ApJS, 199, 19
Guiriec, S., Connaughton, V., Briggs, M. S., Burgess, M., Ryde, F., et al. 2011, ApJL, 727, L33
Guiriec, S., Daigne, F., Hascoët, R., Vianello, G., Ryde, F., et al. 2013, ApJ, 770, 32
Illarionov, A. F., & Siuniaev, R. A. 1975, SvA, 18, 413
Iyyani, S., Ryde, F., Axelsson, M., Burgess, J. M., Guiriec, S., et al. 2013, MNRAS, 433, 2739
Krimm, H. A., Hurkett, C., Pal'shin, V., Norris, J. P., Zhang, B., et al. 2006, ApJ, 648, 1117
Lazzati, D., Morsony, B. J., Margutti, R., & Begelman, M. C. 2013, ApJ, 765, 103
Lightman, A. P. 1981, ApJ, 244, 392
Lloyd-Ronning, N. M., & Zhang, B. 2004, ApJ, 613, 477
Lyutikov, M., & Blandford, R. 2003, arXiv:astro-ph/0312347
Mészáros, P. 2006, RPPh, 69, 2259
Mészáros, P., & Rees, M. J. 2011, ApJL, 733, L40
Narayan, R., McKinney, J. C., & Farmer, A. J. 2007, MNRAS, 375, 548
Novikov, I. D., & Thorne, K. S. 1973, in Black Holes (Les Astres Occlus), ed. C. Dewitt, & B. S. Dewitt
Paczynski, B. 1986, ApJL, 308, L43
Paczynski, B. 1990, ApJ, 363, 218
Pe'er, A. 2008, ApJ, 682, 463
Pe'er, A., Mészáros, P., & Rees, M. J. 2005, ApJ, 635, 476
Pe'er, A., Mészáros, P., & Rees, M. J. 2006, ApJ, 642, 995
Pe'er, A., Ryde, F., Wijers, R. A. M. J., Mészáros, P., & Rees, M. J. 2007, ApJL, 664, L1
Pe'er, A., Zhang, B.-B., Ryde, F., McGlynn, S., Zhang, B., et al. 2012, MNRAS, 420, 468
Piran, T., Shemi, A., & Narayan, R. 1993, MNRAS, 263, 861
Pozdnyakov, L. A., Sobol, I. M., & Syunyaev, R. A. 1983, ASPRv, 2, 189
Rees, M. J., & Meszaros, P. 1992, MNRAS, 258, 41P
Rees, M. J., & Meszaros, P. 1994, ApJL, 430, L93
Rybicki, G. B., & Lightman, A. P. 1979, Radiative Processes in Atrophysics (New York: Wiley-Interscience)
Ryde, F., Axelsson, M., Zhang, B. B., McGlynn, S., Pe'er, A., et al. 2010, ApJL, 709, L172
Ryde, F., & Pe'er, A. 2009, ApJ, 702, 1211
Sironi, L., & Spitkovsky, A. 2014, ApJL, 783, L21
Spruit, H. C., Daigne, F., & Drenkhahn, G. 2001, A&A, 369, 694
Spruit, H. C., & Drenkhahn, G. D. 2004, in ASP Conf. Ser. 312, Gamma-Ray Bursts in the Afterglow Era, ed. M. Feroci et al. (San Francisco, CA: ASP), 357
Svensson, R. 1984, MNRAS, 209, 175
Tchekhovskoy, A., McKinney, J. C., & Narayan, R. 2008, MNRAS, 388, 551
Tchekhovskoy, A., McKinney, J. C., & Narayan, R. 2009, ApJ, 699, 1789
Tchekhovskoy, A., Narayan, R., & McKinney, J. C. 2010, NewA, 15, 749
Thompson, C., Mészáros, P., & Rees, M. J. 2007, ApJ, 666, 1012
Vurm, I., Lyubarsky, Y., & Piran, T. 2013, ApJ, 764, 143
Zhang, B. 2014, IJMPD, 23, 30002
Zhang, B., & Pe'er, A. 2009, ApJL, 700, L65